A form-finding strategy for magneto–elastic actuators.

Jacopo Ciambella[a], Giuseppe Tomassetti[b]

[a] *Dipartimento di Ingegneria Strutturale e Geotecnica, Sapienza Università di Roma, Roma 00184, Italy*
[b] *Dipartimento di Ingegneria, Università Roma Tre, Via Vito Volterra 62, Roma 00146, Italy*

Abstract

We study the inverse problem which arises when designing thin magneto-elastic actuators with bespoken deformation modes. By using the nonlinear model of magneto-elastic rods which we have recently proposed, we formulate the design problem as a PDE-constrained minimization whose solution gives to the optimal distribution of the magnetization profile necessary to achieve the desired shape. The same problem is extended to control multiple deformed configurations which would allow a controlled motion of the actuator to be realised.

Keywords: Inverse problems, Magnetic actuation, Euler's Elastica, PDE-constrained optimization

Todo list

1. Introduction

Magnetic fields are widely used for actuation purposes due to their two main peculiarities: they can operate in the absence of contact and, at low frequency, are essentially harmless to biological tissues [1]. At small scales, shape-programmable magnetic materials could potentially achieve mechanical functionalities that are unattainable by other type of functional materials [2].

From the theoretical side, an interest in the mathematical modelling of magnetoelastic materials, which dates back to the early works of Brown, Tiersten, and Toupin [3, 4, 5], was renewed with the discovery of the huge magnetostriction effect and magnetostrictive shape-memory alloys [6, 7]. For some recent account we refer to [8] or [9, 10]. The subject received further interest with the introduction of the so-called magneto-rheological soft-composite or Magneto-Rheological Elastomers (MRE). These materials, obtained by dispersing magnetic hard particles into a non-magnetic soft matrix, make it possible to manufacture compliant devices that respond to applied fields by either magnetostriction or by magnetic forces and couples, and are widely used as sensors and actuators [11, 12, 13]. Their properties can be finely tuned by controlling during the production

Email addresses: jacopo.ciambella@uniroma1.it (Jacopo Ciambella), giuseppe.tomassetti@uniroma3.it (Giuseppe Tomassetti)

Author's final version accepted for International Journal of NonLinear Mechanics February 21, 2020

phase, the dispersion of the magnetic particles in terms of orientation, dimension and volume fraction. Indeed, the orientation of the particles can be tuned by applying a spatially uniform magnetic field before the curing process of the elastomeric matrix is concluded. This working principle holds for para- and diamagnetic inclusions, as well as ferromagnetic inclusions. In fact, under the influence of the external field, para- and diamagnetic particles become magnetized along a direction not aligned with the field; this mismatch produces a torque which, in turn, makes the particle rotates and aligns with the field lines [14]. On the other hand, if the embedding particles are ferromagnetic, the magnetization can be imprinted permanently upon the application of a sufficiently high field, with the further advantage being able to control the magnetization profile after the specimen is cured and the matrix has become solid.

Recently in [15, 16, 17], a different fabrication technique was used to control both orientation and intensity of the magnetization profile. A mixture of magnetically active neodynium-iron-boron particles and inactive aluminium powder was used to reinforce a silicon rubber. By tailoring the ratio between the active and inactive components the desired magnetization intensity was obtained. The additional control offered by this technique allows very complex actuation mechanisms to be realised including tiny robots that crawl, swim and even jump [17].

Be as it may, there is very large availability of filler types and shapes to be used in MRE, which provides a much larger "design space" compared with other types of soft actuators. As evidence show, technology is mature to produce such devices, with the use, for example, of multi-material 3D printers, which make it possible to embed magnetic fibers in soft matrix to produce regular structures [19]. In addition, it is now possible to realize self-assembled structures made of magnetic spheres or particles, which make it possible to obtain ordered structures [20, 21]. Of course, exploiting such freedom demands substantial understanding of the underlying mechanics. Such understanding must progress along two parallel lines: on one hand, one must rely on the continuum theory of magnetoelasticity, a topic that by now seems to be well established [22, 23, 24**?**]. On the other hand it is quite important in this setting to understand how the micro geometry of the composite affects the overall macroscopic response [25, 26, 27**?**].

Among all possible shapes, magneto-elastic actuators have been mainly crafted in the shape of thin beams. This configuration is indeed particularly efficient in storing and releasing elastic energy. In fact, if ℓ the length of the beam with, say, cross section of diameter $\varepsilon\ell$, with $\varepsilon << 1$, the elastic energy stored in the body obeys the scaling law

$$\text{strain energy} \approx (\varepsilon\ell)^4\kappa^2\ell, \tag{1}$$

where κ is the curvature of the axis. Since the volume of the body is $\varepsilon^2\ell^3$, the specific energy density scales as

$$\frac{\text{strain energy}}{\text{volume}} \approx (\varepsilon\ell)^2. \tag{2}$$

Thus, if we use curvature as a measure of shape changes, we see that for a thin rod the specific energy needed to attain a certain deformation converges to zero as the length tends to null. For a bulky sample, on the other hand, the energy needed to attain a given shape change is size independent. This explains why small thin rods have been employed so much in the context of magnetic actuation. Indeed, rod-shaped magnetic devices have been succesfully used to manufacture flexible swimmers and surface walkers [28, 16], and

their performance has been the subject of several theoretical investigations [29, 30].

A fundamental problem to be addressed, however, is to optimize these objects to achieve maximum actuation or to control their motion with sufficient accuracy. An investigation of how to maximize the displacement of a magnetoelastic rod under an applied field can be found in [31]. Both theoretical and experimental investigations have been carried out in [15, 16]. Indeed, the problem of designing an object having in mind a target shape, even in a wider context, is obtaining more and more attention, and a diversity of approaches are being proposed (see for example the approach proposed in [32] to the design stretch fields in nematic glass sheets).

Magnetoelastic rods. To illustrate how the applied field determines the shape of a rod-like body, let us consider the cantilever beam sketched in Fig. 1 below. The figure shows the beam in its undeformed configuration (left), along with the typical deformed configuration attained when a constant magnetic field is applied (right).

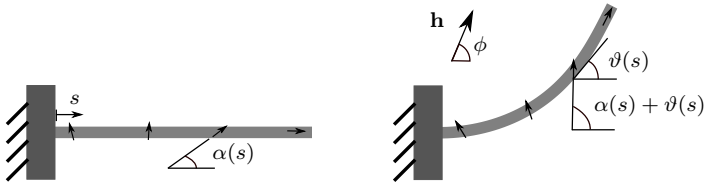

Figure 1: Left: undeformed configuration of a magneto-elastic rod in a cantilever configuration. Right: deformed configuration under the influence of the external, spatially constant, magnetic field **h**. Here s denotes the dimensionless coordinate, $\alpha(s)$ is the local orientation of the magnetization profile and $\theta(s)$ the rotation of the cross-section at s.

fig:1

Let ℓ be the length of the rod. We introduce a dimensionless coordinate s whose domain of definition is $(0,1)$, so that $\vartheta(s)$ is the rotation of the cross section whose arc-length distance from the clamp is $X_1 = s\,\ell$.

After working out the energetics of the magnetoelastic rod (see Section 2), we find an energy functional whose smooth stationary points are solutions of the *state system:*

$$\begin{cases} -\vartheta''(s) + h_x m(s)\sin(\vartheta(s)+\alpha(s)) - h_y m(s)\cos(\vartheta(s)+\alpha(s)) = 0, & \text{in } (0,1), \\ \vartheta(0) = 0, \\ \vartheta'(1) = 0. \end{cases} \tag{3}$$

eq:2b

Here the constants

$$h_x = h\cos(\phi), \qquad h_y = h\sin(\phi), \tag{4}$$

eq:29

with $h > 0$ and $\phi \in [0, 2\pi)$ are the components of the applied field (see Fig. 1); $m(s)$ is a dimensionless field representing the (adimensionalized) magnetization per unit length satisfying

$$m(s) > 0, \qquad \max_s m(s) = 1; \tag{5}$$

eq:22

the angle $\alpha(s) \in \mathbb{R}$ [1] is the orientation of the magnetization in the reference configuration

[1] As we shall see later, not only α, but also its derivative is to be taken into consideration. For this

at the cross section parametrized by s.

We have shown in [33] that there exist choices of α, m, h and ϕ which make (3) identical to the boundary-value problem that governs the equilibrium of a clamped Elastica subjected to a concentrated force at the tip. As for the Elastica, we cannot expect, in general, that (3) has unique solution. However, numerical evidence from [33] suggests that there exists a *threshold intensity* $h_{\max} > 0$ such that (3) has unique solution whenever $h_x^2 + h_y^2 < h_{\max}^2$, independently on the magnetization profile and on the orientation of the field. The task of estimating $h_{\max}$ (or at least provide a good lower bound) appears nontrivial. For the sake of the current discussion, we just suppose that $h_{\max}$ exists and we call *admissible* any field whose intensity is smaller than $h_{\max}$.

Under the circumstance that the applied field is admissible, the solution $\vartheta(s)$ of (3) is uniquely determined by a *quadruplet u of controls*:

$$u \in \mathcal{U} = \{(\alpha(\cdot), m(\cdot), h_x, h_y) \text{ such that (5) holds}\} \tag{6}$$ eq:21

We denote this solution by $\vartheta_u(s)$ and we call it *the actual shape induced by u*.

A design/control problem. Consider now the problem of designing an admissible control $\overline{u}$ so as to attain a given a *target shape* $\overline{\vartheta}(s)$. If the target shape satisfies the condition

$$\max_{s\in[0,1]} \overline{\vartheta}''(s) \leq h_{\max}, \tag{7}$$ eq:24

there is a trivial solution of this problem. In fact, if we take $\overline{m}(s) = 1$, $\overline{h}_x = \max_{s\in[0,1]} |\overline{\vartheta}''(s)|$, $\overline{h}_y = 0$, and with

$$\overline{\alpha}(s) = -\overline{\vartheta}(s) + \arcsin\left(\overline{\vartheta}''(s)/\overline{h}\right), \tag{8}$$ eq:20

and we set $\overline{u} = (\overline{\alpha}(\cdot), \overline{m}(\cdot), \overline{h}_x, \overline{h}_y)$, then $\overline{u} \in \mathcal{U}$ and

$$-\overline{\vartheta}''(s) + \overline{h}_x \overline{m}(s) \sin(\overline{\vartheta}(s) + \overline{\alpha}(s)) = 0. \tag{9}$$ eq:31

Since the state system has unique solution, we deduce from (9) that the shape $\vartheta_{\overline{u}}(s)$ induced by the control $\overline{u}$ coincides with the target shape $\overline{\vartheta}(s)$:

$$\vartheta_{\overline{u}}(s) = \overline{\vartheta}(s). \tag{10}$$

Once the magnetization profile has been imprinted in the rod, the only control that we have at our disposal to affect its motion is the applied magnetic field. Thus, if instead of a single shape we are given a list $(\overline{\vartheta}_i(s))_{i=1}^N$ of target shapes, the most we can do is to look for a magnetization profile $(m(s), \alpha(s))$ and a list of N applied fields $(h_{xi}, h_{yi})_{i=1}^N$ such that the list of shapes $\{\theta_{i_n}(s)\}_{i=1}^N$ induced by the controls $(u_i)_{i=1}^N = (\alpha(\cdot), m(\cdot), h_{xi}, h_{yi})_{i=1}^N$ is as close as possible, in a suitable sense, to the list of target shapes.

Needless to say, the solution of this problem depends on how, given a control u, we define the error $E(u, \overline{\vartheta})$ in the attainment of the target shape $\overline{\vartheta}(s)$ by the shape $\vartheta_u(s)$.

reason, we prefer to let the range of α be the entire set of real numbers, although functions differing by 2π

What appears to us a reasonable definition of the error is

$$E(u,\overline{\vartheta}) = \int_0^1 (\vartheta_u(s) - \overline{\vartheta}(s))^2 ds, \tag{11}$$ eq:1

namely, the L^2 distance between the attained and the target shape. With this choice, we derive necessary conditions for a control to be a stationary point of the error. We justify the model leading to (3) in Sections 2 and 3. In Section 4 we consider a regularization of the error function and derive the corresponding necessary conditions for optimality. In Section 5 we illustrate an example. Section 6 contains concluding remarks.

2. The magnetoelastic energy

For the reader's convenience, this section summarizes the dimension-reduction procedure carried out in [33]. This presentation is simplified, assuming that the body has a permament magnetization density as per the experiments in [15, 16].

We suppose for simplicity that in the reference configuration the cantilever is a thin strip Ω^ε of length ℓ, width w, and thickness $t^\varepsilon = \varepsilon t$, where ε is a small dimensionless parameter. We assume that the material comprising the body has a permanent magnetization density, whose orientation is given by a field $\boldsymbol{a}$, of unit vectors and whose intensity is a scalar field M. If the magnetization process takes place after curing, we may assume that there is no rearrangement of the magnetic particles in the matrix. Moreover, if the suspension of particles is sufficiently diluted, there is no mutual interaction and from the mechanical standpoint the material is mechanically isotropic.

To describe the deformation of the strip, we introduce a coordinate system $\boldsymbol{X} = (X_1, X_2, X_3)$, and we let $\{\boldsymbol{c}_1, \boldsymbol{c}_2, \boldsymbol{c}_3\}$ be the associated orthonormal basis. We restrict attention to deformations that take place on the plane spanned by $\boldsymbol{c}_1$ and $\boldsymbol{c}_2$ and, owing to the assumption of small thickness we suppose that the deformation is linear with respect to the thickness coordinate:

$$\boldsymbol{f}(\boldsymbol{X}) = \boldsymbol{r}(X_1) + X_2 \boldsymbol{d}(X_1). \tag{12}$$ defrod

The vectors $\boldsymbol{r}(X_1)$ and $\boldsymbol{d}(X_1)$ represent, respectively, the position and the orientation of the typical *cross section* $X_1 \in (0, \ell)$. We rule out axial extension and shear by requiring that

$$|\boldsymbol{r}'| = 1, \quad \boldsymbol{d} = \boldsymbol{c}_3 \times \boldsymbol{r}' \tag{13}$$ eq:6

where a prime denotes differentiation with respect to the coordinate X_1. We write the strain energy of the body as

$$\mathcal{E}_{\rm s} = \int_{\Omega^\varepsilon} \widehat{\psi}_{\rm el}(\nabla \boldsymbol{f}(\boldsymbol{X})) d\boldsymbol{X}, \tag{14}$$ eq:5

where the deformation gradient is

$$\nabla \boldsymbol{f}(\boldsymbol{X}) = (1 - \kappa X_2)\boldsymbol{r}' \otimes \boldsymbol{c}_1 + \boldsymbol{d} \otimes \boldsymbol{c}_2 + \boldsymbol{c}_3 \otimes \boldsymbol{c}_3, \tag{15}$$ eq:2

where $\kappa = \boldsymbol{r}'' \cdot \boldsymbol{d}$ is the *signed curvature* of the axis. Without loss of generality, we assume that $\widehat{\psi}_{\rm el}(\boldsymbol{I}) = 0$ and that the reference configuration is stress–free, so that $\partial_{\boldsymbol{F}} \widehat{\psi}_{el}(\boldsymbol{I}) = \boldsymbol{0}$.

By performing a Taylor expansion with respect to X_2 of the integrand in (14) we arrive at (we refer to [33] for additional details):

$$\mathcal{E}_{\rm s}(\boldsymbol{f}) = \frac{\varepsilon^3}{2}\int_0^\ell EI\kappa^2 {\rm d}X_1 + o(\varepsilon^3), \quad \text{with} \quad I = \frac{wt^3}{12}, \tag{16}$$ psiel

where $E = \partial^2_{\boldsymbol{F}\boldsymbol{F}}\widehat{\psi}_{el}(\boldsymbol{I})[\boldsymbol{c}_1\otimes\boldsymbol{c}_1]\cdot\boldsymbol{c}_1\otimes\boldsymbol{c}_1$.

Since the magnetization of the embedded particles is permanent, and since these particles are firmly embedded in the matrix, the orientation of the magnetization in the deformed configuration is

$$\boldsymbol{a}^c(\boldsymbol{F}) = \frac{\boldsymbol{F}(\boldsymbol{X})\boldsymbol{a}(\boldsymbol{X})}{|\boldsymbol{F}(\boldsymbol{X})\boldsymbol{a}(\boldsymbol{X})|}, \qquad \boldsymbol{F} = \nabla\boldsymbol{f}, \tag{17}$$ eq:12

and the interaction energy with the external applied field $\mathbf{h}^\varepsilon$ is

$$\mathcal{E}_{\rm m}(\boldsymbol{f}) = -\int_{\Omega^\varepsilon} M(\boldsymbol{X})\,\mathbf{h}^\varepsilon(\boldsymbol{f}(\boldsymbol{X}))\cdot\boldsymbol{a}^c(\nabla\boldsymbol{f}(\boldsymbol{X}))\,d\boldsymbol{X}. \tag{18}$$ eq:7

The polar decomposition of the deformation gradient $\boldsymbol{F} = \nabla\boldsymbol{f}$ is

$$\boldsymbol{F}(\boldsymbol{X}) = \boldsymbol{R}(\boldsymbol{r}'(X_1))\boldsymbol{U}(X_1, X_2), \tag{19}$$ eq:3-3

with

$$\boldsymbol{R}(\boldsymbol{r}') = \boldsymbol{r}'\otimes\boldsymbol{c}_1 + (\boldsymbol{c}_3\times\boldsymbol{r}')\otimes\boldsymbol{c}_2 + \boldsymbol{c}_3\otimes\boldsymbol{c}_3 \qquad \text{and} \qquad \boldsymbol{U} = \boldsymbol{I} - \kappa X_2\boldsymbol{c}_1\otimes\boldsymbol{c}_1. \tag{20}$$ eq:11

By (19) and by the second of (13),

$$\boldsymbol{a}^c(\nabla\boldsymbol{f}) = \boldsymbol{R}(\boldsymbol{r}')\boldsymbol{a}. \tag{21}$$ eq:4

Moreover,

$$\mathbf{h}^\varepsilon(\boldsymbol{f}(\boldsymbol{X})) = \mathbf{h}^\varepsilon(\boldsymbol{r}(X_1)) + X_2\boldsymbol{g}(\boldsymbol{X}), \tag{22}$$ eq:8

where $\boldsymbol{g}(\boldsymbol{X})$ is a bounded function. Starting from (18), and making use of (21) and (22), and assuming that the magnetic field scales as

$$\mathbf{h}^\varepsilon = \varepsilon^2\mathbf{h}, \tag{23}$$

we obtain

$$\mathcal{E}_{\rm m} = -\varepsilon^3\int_0^\ell \boldsymbol{R}(X_1)\boldsymbol{m}(X_1)\cdot\mathbf{h}\,dX_1 + o(\varepsilon^3), \tag{24}$$

where $\boldsymbol{m}(X_1) = \int_{-w/2}^{+w/2}\int_{-t/2}^{+t/2} M(\boldsymbol{X})\boldsymbol{a}(\boldsymbol{X})dX_2dX_3$ it the magnetization per unit length taken along the axis.

The total energy is the difference between the strain and magnetostatic energy. If no external loads are present, we can rescale the energy by ε^3 without loss of generality and

neglect higher-order terms in ε, to obtain

$$\widetilde{\mathcal{E}} = \frac{\mathcal{E}_{\rm s} + \mathcal{E}_{\rm m}}{\varepsilon^3} = \int_0^\ell \left[\frac{EA}{2} (\boldsymbol{r}'')^2 - \boldsymbol{R}(\boldsymbol{r}')\boldsymbol{m} \cdot \mathbf{h} \right] dX_1, \tag{25}$$ eq:13

which is of the same form of the energy proposed in [33] but with constant magnetization.

3. Cantilever beam under constant applied field.

For a cantilever beam, we take into account the clamping constrain at $X_1 = 0$ by requiring that $\boldsymbol{r}(X_1) = \mathbf{0}$ and $\boldsymbol{r}'(X_1) = \boldsymbol{c}_1$. In this case, it is convenient to parametrize the the configuration of the axis $\boldsymbol{r}(X_1)$ through the rotation field $\theta(X_1)$ such that

$$\boldsymbol{r}'(X_1) = \cos\theta(X_1)\boldsymbol{c}_1 + \sin\theta(X_1)\boldsymbol{c}_2, \tag{26}$$ eq:10

then, the rotation $\boldsymbol{R}(\boldsymbol{r}')$ introduced in (20) can be written as a the following 3-by-3 matrix

$$\boldsymbol{R}(\boldsymbol{r}') = \mathbf{R}(\theta) = \begin{pmatrix} \cos\theta & \sin\theta & 0 \\ -\sin\theta & \cos\theta & 0 \\ 0 & 0 & 1 \end{pmatrix}. \tag{27}$$

If the applied magnetic field $\mathbf{h} = (h_x, h_y)$ is constant, the magnetoelastic energy (25) yields

$$\widetilde{\mathcal{E}} = \int_0^\ell \left[\frac{EA}{2} \theta'^2 - \mathbf{R}(\theta)\boldsymbol{m} \cdot \mathbf{h} \right] dX_1. \tag{28}$$

We shall find it convenient to work with dimensionless variables. To this effect, we define $M = \max_{X_1 \in [0,\ell]} |\boldsymbol{m}(X_1)|$, the rescaled coordinate axis

$$s = X_1/\ell,$$

the renormalized magnetization density $m(s) = |m(X_1)|/M$, and the renormalized magnetic-field intensity $h = A\ell^2|\boldsymbol{h}|M/(EI)$, and the rotation $\vartheta(s) = \theta(\ell s)$. Then on denoting by $\alpha(s)$ the angle between the horizontal direction and the magnetization vector $\boldsymbol{m}(\ell s)$, we have

$$\boldsymbol{m}(X_1) = Mm(X_1/\ell)\mathbf{R}(\alpha(X_1/\ell))\boldsymbol{c}_1. \tag{29}$$

Likewise, on denoting by ϕ the angle between the horizontal direction and the applied field,

$$\mathbf{h} = h\boldsymbol{R}(\phi)\boldsymbol{c}_1. \tag{30}$$

Accordingly,

$$\mathbf{R}(\theta)\boldsymbol{m} \cdot \mathbf{h} = \frac{EI}{A\ell^2} hm\mathbf{R}(\vartheta + \alpha - \phi)\boldsymbol{c}_1 \cdot \boldsymbol{c}_1 = \frac{EI}{A\ell^2} hm\sin(\vartheta + \alpha - \phi). \tag{31}$$

On setting $\mathcal{E} = \widetilde{\mathcal{E}} \frac{A\ell^2}{EI}$ we obtain

$$\mathcal{E} = \int_0^1 \Big[\frac{\vartheta'^2(s)}{2} - h\, m(s)(\cos(\vartheta(s) + \alpha(s) - \phi) \Big] ds. \tag{32}$$ eq:3

With the position (4), on making $\mathcal{E}$ stationary with respect to ϑ, we obtain the first and the third of (3).

4. The optimization problem

Before formulating the optimization problem, we recall its informal statement, which we were alluding at in the end of the introduction:

- given a list of N *target shapes*:

$$\overline{\boldsymbol{\vartheta}}(s) = (\overline{\vartheta}_i(s))_{i=1}^N,$$

  design

  - a *magnetization profile* $(m(s), \alpha(s))$ (i.e., the intensity and the orientation of the magnetization) and
  - a list of *applied fields*

$$\boldsymbol{h} = (h_{xi}, h_{yi})_{i=1}^N$$

  such that the *state system*:

$$\begin{cases} -\vartheta_i'' + m\, h_{xi} \sin(\vartheta_i + \alpha) - m\, h_{yi} \cos(\vartheta_i + \alpha) = 0 \quad \text{in } (0,1), & i = 1 \dots N, \\ \vartheta_i(0) = 0, & i = 1 \dots N, \\ \vartheta_i'(1) = 0, & i = 1 \dots N, \end{cases} \tag{33}$$

  admits a list of solutions $\boldsymbol{\vartheta}(s) = (\vartheta_i(s))_{i=1}^N$ which is as close as possible to the desired list $\overline{\boldsymbol{\vartheta}}(s) = (\overline{\vartheta}_i(s))_{i=1}^N$ of "target"functions.

As a first step, we define the *shape distance*:

$$D(\boldsymbol{\vartheta}, \overline{\boldsymbol{\vartheta}}) = \sum_{i=1}^{n} \int_0^1 |\vartheta_i - \overline{\vartheta}_i|^2 ds\,. \tag{34}$$

and the *cost functional*:

$$\mathcal{C}(\boldsymbol{\vartheta}, \alpha, m, \mathbf{h}) = \frac{W}{2} D(\boldsymbol{\vartheta}, \overline{\boldsymbol{\vartheta}}) + \mathcal{R}(\alpha, m, \boldsymbol{h}), \tag{35}$$

where W is a *tuning weight* and

$$\mathcal{R}(\alpha, M, \boldsymbol{h}) = \int_0^1 \left(\frac{\varepsilon}{2} \alpha'^2 + \frac{\gamma}{2} m^2 \right) ds + \frac{\widetilde{\gamma}}{2} \sum_{i=1} (h_{xi}^2 + h_{yi}^2), \tag{36}$$

is a *regularization* function dependent on the positive *tuning parameters* ε, γ, and $\widetilde{\gamma}$.

The design of the actuator is formulated as an ODE constrained minimization of the cost functional $\mathcal{C}(\boldsymbol{\vartheta})$ under the constraint that the functions ϑ_i which form the vector $\boldsymbol{\vartheta}$ solve the *state equation* (33), that is to say, we look for the solution of the following

problem:

$$\boxed{\begin{array}{l}\text{minimize } \mathcal{C}(\boldsymbol{\vartheta},\alpha,m)\\ \text{with respect to } (\boldsymbol{\vartheta},\alpha,m,\boldsymbol{h}),\\ \text{subject to (33). } \boxed{\texttt{eq:14}}\end{array}} \tag{37}$$ eq:14

It is important to stress that if a list $(\boldsymbol{\vartheta},\alpha,m,\boldsymbol{h})$ is a solution of (37), then $\boldsymbol{\vartheta}$ does not minimize the function $D(\cdot,\overline{\boldsymbol{\vartheta}})$, because of the presence of the regularization function (36) in the definition (35) of the cost. The introduction of the regularization function serves the purpose of making the minimization problem well posed, and the choice of a quadratic regularization is for analytical convenience (see, for instance, [35] or [36]). On the other hand, we expect that if the regularization parameters are sufficiently small, then the effect of the regularization will be minimal. This point will be further discussed in the next section.

As a first step towards an understanding of (37), we write down the necessary conditions that a solution must satisfy, by introducing a list of Lagrange multipliers $\boldsymbol{\lambda}(s)=(\lambda_i(s))_{i=1}^N$, and by considering the Lagrangean

$$\mathcal{L}(\boldsymbol{\vartheta},\alpha,m,\boldsymbol{h},\boldsymbol{\phi},\boldsymbol{\lambda})=\mathcal{C}(\boldsymbol{\theta},\alpha,m)-\sum_{i=1}^{N}\int_0^1\lambda_i\left(-\vartheta_i''+mh_{xi}\sin(\vartheta_i+\alpha)-mh_{yi}\cos(\vartheta_i+\alpha)\right)ds. \tag{38}$$ eq:23

The stationarity conditions for $\mathcal{L}$ lead to a set of differential-algebraic equations:

$$\begin{aligned}
&-\vartheta_i''+mh_{xi}\sin(\vartheta_i+\alpha)-mh_{yi}\cos(\vartheta_i+\alpha)=0, \qquad i=1\dots n,\\
&-\lambda_i''+W(\vartheta_i-\overline{\vartheta}_i)-\lambda_i(mh_{xi}\cos(\vartheta_i+\alpha)+mh_{yi}\sin(\vartheta_i+\alpha))=0, \qquad i=1\dots n,\\
&-\varepsilon\alpha''-\sum_i\left[mh_{xi}\cos(\vartheta_i+\alpha)+mh_{yi}\sin(\vartheta_i+\alpha)\right]=0,\\
&\gamma m-\sum_i\lambda_i(h_{xi}\sin(\vartheta_i+\alpha)-h_{yi}\cos(\vartheta_i+\alpha))=0,\\
&\widetilde{\gamma}h_{xi}-\int_0^1\lambda_i m\sin(\vartheta_i+\alpha)ds=0,\\
&\widetilde{\gamma}h_{yi}+\int_0^1\lambda_i m\cos(\vartheta_i+\alpha)ds=0,
\end{aligned} \tag{39}$$ eq:15

with the two-point conditions:

$$\begin{aligned}
&\vartheta_i(0)=0, \qquad &&\vartheta_i'(1)=0,\\
&\lambda_i(0)=0, \qquad &&\lambda_i'(1)=0,\\
&\alpha_i'(0)=0, \qquad &&\alpha_i'(1)=0.
\end{aligned} \tag{40}$$

The last two optimality conditions in (39) are linear with respect to the components of the applied fields. In the next section we discuss examples where the optimality conditions (in particular, the first four of (39)) are used to devise an optimal design.

5. Examples

We have pointed out in the previous section (see the paragraph following (37)) that the solution of the minimization problem (37) does not necessarily render minimal the distance between the actual shape and the target shape. We have also pointed out in the introduction of this paper, that when there is only a single target shape $\overline{\vartheta}(s)$, the optimal design problem has an explicit solution, in the sense that we have an explicit formula for a control $(\overline{\alpha}, \overline{m}, \overline{h}_x, \overline{h}_y)$ whose induced shape $\vartheta_{\overline{u}}(s)$ coincides with the target $\overline{\vartheta}(s)$. It is then natural for us to use this analytical solution as a benchmark to assess the performance of the minimization problem as an optimal design tool. Accordingly, in our first example, we consider problem of designing the actuator to attain a single shape and we work out a comparison between the control $\overline{u}$ and the control produced by the minimization problem (37).

The minimization problem (37) formulated for $N = 1$ has the list of functions $\overline{\boldsymbol{\vartheta}}(s)$ composed of the single target shape function $\overline{\vartheta}(s)$ and can be written as

$$\boxed{\begin{array}{l}\text{minimize } \mathcal{C}(\vartheta, \alpha, m)\\ \text{with respect to } (\vartheta, \alpha, m, h_x, h_y),\\ \text{subject to (3).} \quad \texttt{eq:14b}\end{array}} \tag{41}$$ eq:14b

with the distance function given by

$$D(\vartheta, \overline{\vartheta}) = \int_0^1 |\vartheta(s) - \overline{\vartheta}(s)|^2 ds. \tag{42}$$

Here, we make the following choice for the target shape:

$$\overline{\vartheta}(s) = A \sin\left(\frac{\pi}{2} s\right), \qquad A > 0. \tag{43}$$ singleshape

This shape is similar to what is proposed in [16] to mimic an artificial cilium. Arguing as in the introduction, we observe that $\overline{\vartheta}(s)$ is the solution of the boundary value problem

$$\begin{cases} -\overline{\vartheta}'' + \overline{h}_x \sin(\overline{\vartheta} + \overline{\alpha}) = 0 \quad \text{in } (0,1),\\ \vartheta(0) = 0,\\ \vartheta'(1) = 0, \end{cases} \tag{44}$$ eq:9

where

$$\overline{h}_x = \left(\frac{\pi}{2}\right)^2 A, \qquad \overline{\alpha}(s) = -\frac{\pi}{2} s - A \sin\left(\frac{\pi}{2} s\right). \tag{45}$$

Accordingly, the shape $\vartheta_{\overline{u}}(s)$ induced by the control $\overline{u} = (\overline{\alpha}, \overline{m}, \overline{h}_x, 0)$ coincides with $\overline{\vartheta}(s)$. This is equivalent to saying that the list $(\overline{\vartheta}, \overline{\alpha}, 1, \overline{h}_x, 0)$ is solution of the following minimization problem

$$\boxed{\begin{array}{l}\text{minimize } \mathcal{D}(\vartheta, \overline{\vartheta})\\ \text{with respect to } (\vartheta, \alpha, m, h_x, h_y),\\ \text{subject to (44).} \quad \texttt{eq:14c}\end{array}} \tag{46}$$ eq:14c

Initialisation:
  TOL $= 0.01$, $\alpha_0 = \overline{\alpha}(s)$, $m_0 = 1$, $h_{x\,0} = \overline{h}_x$, $h_{y\,0} = 0$;
  SET $\{W, \varepsilon, \gamma, \tilde{\gamma}\}$;
  $C_{cur} = 1$;
repeat
  $(\vartheta_1, h_{x\,1}, h_{y\,1}) = \text{argmin}_{(\vartheta, h_x, h_y)} \mathcal{C}(\vartheta, \alpha_0, m_0)$, subjected to Eq. (3) with $h_{x\,0}$ and $h_{y\,0}$ initial points of the minimization algorithm;
  $(\vartheta_2, \alpha, m) = \text{argmin}_{(\vartheta, \alpha, m)} \mathcal{C}(\vartheta, \alpha, m)$, subjected to Eq. (3) with $h_x = h_{x\,1}$ and $h_y = h_{y\,1}$;
  $\alpha_0 = \alpha$, $m_0 = m$, $h_{x\,0} = h_{x\,1}$ and $h_{y\,0} = h_{y\,1}$;
  $C_{prev} = C_{cur}$;
  $C_{cur} = \mathcal{C}(\vartheta_2, \alpha, m)$;
until $|C_{cur} - C_{prev}| >$ TOL;

Figure 2: Numerical algorithm used to solve (39) for the single-shape problem. fig:algo

A more accurate control over the magnetization profile is obtained by solving (41) and adjusting the control parameters $\{W, \varepsilon, \gamma, \tilde{\gamma}\}$ (see Eq. (36)). In doing so, much care must be taken to avoid of being be trapped in a local minimum due to the highly nonlinear character of the functional $\mathcal{C}$. For such a reason, we use an alternate minimization strategy made of the following two stages:

1. in the first stage, the magnetic fields that minimize (41) with α and m kept fixed are found;
2. in the second stage, the minimization is carried out in terms of α, m and λ with values of the magnetic field h_x and h_y found at previous step.

The initial guess for the minimization algorithm, which constitutes a crucial choice in this kind of nonlinear problems, is the solution $\overline{u}$ of (46) (see Fig. 2 for schematic description of the algorithm). In implementing the algorithm in MATLAB, rather than carrying out the minimization over an infinite dimensional space, we solve the associated BVP problem given by Eqs $(39)_{1\text{-}4}$.

The control parameters $\{W, \varepsilon, \gamma, \tilde{\gamma}\}$ in (35)-(36) can be tuned to improve the solution achieved. In this respect, Fig. 3 shows two numerical solutions of the minimization problem (41) obtained for different choices of these control parameters. The deformation of the actuator is remarkably close to the desired shape which is represented by the red dashed curve in insets (a), (b) and (c); however, the magnetization profile is quite different for the three solutions: the yellow curve corresponds to the set of control parameters given by $\{W, \varepsilon, \gamma, \tilde{\gamma}\} = \{200, 0.05, 100, 0.01\}$ which penalizes the variation of the magnetization intensity rather than its orientation this is why the resulting magnetization profile is essentially constant. On the opposite, by penalising α' with the choice $\{W, \varepsilon, \gamma, \tilde{\gamma}\} = \{300, 0.15, 3, 0.005\}$, one obtains the solution represented by the green curve, for which the orientation profile is constant but significant variations of the magnetization intensity are observed.

Still with reference to the profile of the magnetization orientation shown in Fig. 3, we observe the smoothening effect of the regularization parameter ε. Indeed, the profile that gives the magnetization orientation of the numerical solution (blue curve), appears as a "regularization" of the magnetization orientation $\overline{\alpha}(s)$ given from the explicit solution (orange curve). We also notice that $\overline{\alpha}'(0) \neq 0$ and $\overline{\alpha}'(1) \neq 0$.

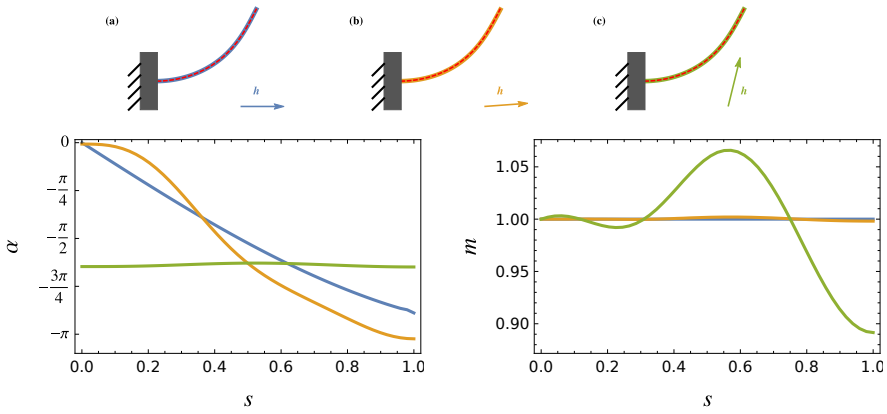

Figure 3: Results of the optimization procedure for the single shape problem with $\overline{\vartheta}$ in (43). (left) magnetization orientation, (right) magnetization intensity for the three solutions considered: (a) represents the solution of (46), (b) and (c) are the solution of (41) with $\{W, \varepsilon, \gamma, \tilde{\gamma}\} = \{200, 0.05, 100, 0.01\}$ and $\{W, \varepsilon, \epsilon, \tilde{\gamma}\} = \{300, 0.15, 3, 0.005\}$, respectively. The coloured arrows indicate the orientation of the magnetic field.

fig:2

The possibility of tuning the control parameter to achieve different types of solutions is indeed beneficial to the experimentalists and in fact the possibility of mutually control the magnetization intensity and the orientation can be exploited to obtain multiple complex shapes [17]. For instance, mimicking an artificial cilium capable of propelling small objects in a fluid-like environment requires at least two shapes to be defined. For this purpose, we introduce two target shapes:

$$\overline{\vartheta}_1(s) = A\sin(3\pi/2s), \qquad \overline{\vartheta}_2(s) = -A\sin(\pi/2s). \tag{47}$$

targetshapes

These shapes represent, respectively, the upward and backward configurations of a cilium Accordingly, we now have to solve the minimization problem (37) with $N = 2$. The results of the optimization algorithm with $\{W, \varepsilon, \gamma, \tilde{\gamma}\} = \{200, 0.05, 100, 0.01\}$ are shown in Fig. 4 together with the corresponding orientation of the magnetic field associated to each configuration. In particular, the results of the minimum of the problem is achieved when $\mathbf{h}_1 = (h_{x1}, h_{y1}) = (13.2, 2.2)$ (configuration (a) in Fig. 4) and $\mathbf{h}_2 = (h_{x2}, h_{y2}) = (-1.3, -7.4)$ (configuration (b)).

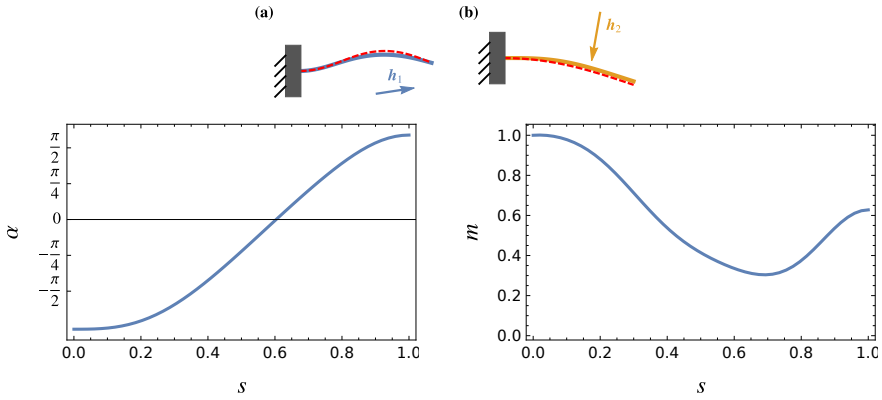

Figure 4: Results of the optimization procedure for 2-shapes problem with $\overline{\vartheta_1}$ and $\overline{\vartheta_2}$ given by Eq. (47). Dashed curves represent the target shapes; solid curves represent the attained shapes. The left graph shows the magnetization orientation, the right one the magnetization intensity. fig:3

We see that in this case the minimization procedure was able to sort out a magnetization profile and applied field whose associated shapes adequately match the targets.

Of course, one may consider solving the problem with even more shapes that interpolate the two targets. However, such interpolation can be obtained by directly interpolating the applied fields that produce the two extreme shapes of the motion. More precisely, a controlled motion of the actuator can be realised by varying the magnetic field between these two extreme configurations through a control parameters $k \in [0, 1]$ as $\mathbf{h}(k) = (1 - k)\,\mathbf{h}_1 + k\,\mathbf{h}_2$. Snapshots of the resulting motion is displayed in Fig. 5. We point out that each configuration of the actuator is the solution of the equilibrium problem (3) with α and m in Fig. 4.

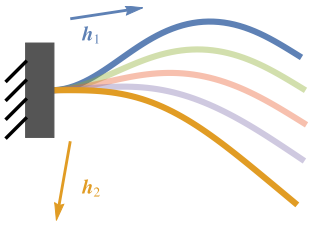

Figure 5: Controlled motion of the actuator obtained by varying the external magnetic between $(h_{x1}, h_{y1}) = (13.2, 2.2)$ and $(h_{x2}, h_{y2}) = (-1.3, -7.4)$. Each shape of the actuator is the solution of the equilibrium problem (3) with α and m in Fig. 4. fig:4

6. Conclusions

In this paper we have considered the problem of steering a magnetized elastic rod towards a sequence of target shapes by the application of a spatially-uniform and possibly time-dependent magnetic field, being free to choose the magnetization profile of the rod.

Since it is not possible to match more than one shape with a given magnetization profile, an optimality criterion must be devised to obtain a good tradeoff. To this effect, we have proposed a new optimality criterion for the design of the magnetization profile, based on a set of optimality conditions drawn from the general theory of PDE-constrained optimization. We have applied this criterion to two benchmark examples. In the first example we have compared what is suggested by our criterion with an explicit analytical solution; in the second example, we have considered the problem of replicating the stroke of an artificial cilium. In both cases, the design criterion shows good performance. This preliminary investigation opens the way to further work to enlarge the space of design variables, by allowing the rod to be tapered, or by allowing the magnetic field to be spatially-inhomogeneous. This design principle could well be extended to other structural models, such as plates and shells.

Acknowledgements

We thank Lorenzo Giacomelli and Riccardo Durastanti for numerous and insightful discussions. GT is supported by the Grant of Excellence Departments, MIUR-Italy (Art.1, commi 314-337, Legge 232/2016). We also thank two anonymous referees for helping us to improve the paper.

References

Rikken2014 [1] Rikken, R. S. M., Nolte, R. J. M., Maan, J. C., Van Hest, J. C. M., Wilson, D. A., & Christianen, P. C. M. (2014). Manipulation of micro- and nanostructure motion with magnetic fields. Soft Matter, 10(9), 1295–1308. https://doi.org/10.1039/c3sm52294f

Chen2017 [2] Chen, X.-Z., Hoop, M., Mushtaq, F., Siringil, E., Hu, C., Nelson, B. J., & Pané, S. (2017). Recent developments in magnetically driven micro- and nanorobots. Applied Materials Today, 9, 37–48. https://doi.org/10.1016/j.apmt.2017.04.006

Brown1966 [3] Brown, W. F. (1966). Magnetoelastic interactions. Springer.

Tiersten1964 [4] Tiersten, H. F. (1964). Coupled magnetomechanical equations for magnetically saturated insulators. Journal of Mathematical Physics, 5(9), 1298–1318. https://doi.org/10.1063/1.1704239

Toupin1956 [5] Toupin, R. A. (1956). The Elastic Dielectric. Arch. Ration. Mech. Anal., 5(6), 849–915. https://www.jstor.org/stable/24900192

Engdahl2000 [6] Engdahl, G., & Mayergoyz, I. D. (2000) Handbook of giant magnetostrictive materials. Elsevier.

Tickle1999 [7] Tickle, R., James, R. D., Shield, T., Wuttig, M., & Kokorin, V. V. (1999). Ferromagnetic shape memory in the NiMnGa system. IEEE Transactions on Magnetics, 35(5), 4301–4310. https://doi.org/10.1109/20.799080

Dorfmann2014 [8] Dorfmann, L., & Ogden, R. W. (2014). Nonlinear Theory of Electroelastic and Magnetoelastic Interactions. Boston, MA: Springer US. https://doi.org/10.1007/978-1-4614-9596-3

Roubicek2013 [9] Roubíček, T., & Tomassetti, G. (2013). Phase Transformations in Electrically Conductive Ferromagnetic Shape-Memory Alloys, Their Thermodynamics and Analysis. Arch. Rat. Mech. Analysis, 213(1), 1–43. https://doi.org/10.1007/s00205-013-0648-2

Roubicek2018 [10] Roubíček, T., & Tomassetti, G. (2018). A thermodynamically consistent model of magneto-elastic materials under diffusion at large strains and its analysis. Zeitschrift Für Angewandte Mathematik Und Physik, 69(3), 55. https://doi.org/10.1007/s00033-018-0932-y

Varga2006 [11] Varga, Z., Filipcsei, G. & Zrínyi, M. Smart composites with controlled anisotropy. Polymer. 46, 7779–7787 (2005).

Erb2016 [12] Erb, R. M., Martin, J. J., Soheilian, R., Pan, C. & Barber, J. R. Actuating Soft Matter with Magnetic Torque. Adv. Funct. Mater. 26, 3859–3880 (2016).

Stanier2016 [13] Stanier, D. C., Ciambella, J., & Rahatekar, S. S. (2016). Fabrication and characterisation of short fibre reinforced elastomer composites for bending and twisting magnetic actuation. Composites Part A: Applied Science and Manufacturing, 91, 168–176. https://doi.org/10.1016/j.compositesa.2016.10.001

Ciambella2017 [14] Ciambella, J., Stanier, D. C. & Rahatekar, S. S. Magnetic alignment of short carbon fibres in curing composites. Compos. Part B Eng. 109, 129–137 (2017).

Sitti2016 [15] Lum, G. Z., Ye, Z., Dong, X., Marvi, H., Erin, O., Hu, W., & Sitti, M. (2016). Shape-programmable magnetic soft matter. Proceedings of the National Academy of Sciences, 113(41), E6007–E6015. https://doi.org/10.1073/pnas.1608193113

Sitti2018 [16] Hu, W., Lum, G. Z., Mastrangeli, M., & Sitti, M. (2018). Small-scale soft-bodied robot with multimodal locomotion. Nature, 554 (7690), 81-85. https://doi.org/10.1038/nature25443

Xu2019 [17] Xu, T., Zhang, J., Salehizadeh, M., Onaizah, O. & Diller, E. Millimeter-scale flexible robots with programmable three-dimensional magnetization and motions. Sci. Robot. 4, eaav4494 (2019).

Fukunaga2008 [18] Fukunaga, A., Urayama, K., Takigawa, T., DeSimone, A., & Teresi, L. (2008). Dynamics of Electro-Opto-Mechanical Effects in Swollen Nematic Elastomers. Macromolecules, 41(23), 9389–9396. https://doi.org/10.1021/ma801639j

Li2018 [19] Li, J., Slesarenko, V., Galich, P. I., & Rudykh, S. (2018). Instabilities and pattern formations in 3D-printed deformable fiber composites. Composites Part B: Engineering, 148(April), 114–122. https://doi.org/10.1016/j.compositesb.2018.04.049

Messina2014 [20] Messina, R., Khalil, L. A., & Stanković, I. (2014). Self-assembly of magnetic balls: From chains to tubes. Physical Review E, 89(1), 011202. https://doi.org/10.1103/PhysRevE.89.011202

idalgo-Caballero2019 [21] Hidalgo-Caballero, S., Escobar-Ortega, Y. Y., Becerra-Deana, R. I., Salazar, J. M., & Pacheco-Vázquez, F. (2019). Mechanical properties of macroscopic magnetocrystals. Journal of Magnetism and Magnetic Materials, 479, 149–155. https://doi.org/10.1016/j.jmmm.2019.02.031

Dorfmann2004 [22] Dorfmann, A. & Ogden, R. W. Nonlinear magnetoelastic deformations of elastomers. Acta Mech. 167, 13–28 (2004).

Kankanala2004 [23] Kankanala, S. V & Triantafyllidis, N. On finitely strained magnetorheological elastomers. J. Mech. Phys. Solids 52, 2869–2908 (2004).

Barham2012 [24] Barham, M., Steigmann, D. J. & White, D. Magnetoelasticity of highly deformable thin films: Theory and simulation. Int. J. Non. Linear. Mech. 47, 185–196 (2012).

Borcea2001 [25] Borcea, L. & Bruno, O. On the magneto-elastic properties of elastomer-ferromagnet composites. J. Mech. Phys. Solids 49, 2877–2919 (2001).

Danas2012 [26] Danas, K., Kankanala, S. V & Triantafyllidis, N. Experiments and modeling of iron-particle-filled magnetorheological elastomers. J. Mech. Phys. Solids 60, 120–138 (2012).

Ethiraj2016 [27] Ethiraj, G. & Miehe, C. Multiplicative magneto-elasticity of magnetosensitive polymers incorporating micromechanically-based network kernels. Int. J. Eng. Sci. 102, 93–119 (2016). https://10.1016/j.ijengsci.2015.08.007

Kimura2012 [28] Kimura, T., Umehara, Y., & Kimura, F. (2012). Magnetic field responsive silicone elastomer loaded with short steel wires having orientation distribution. Soft Matter, 8(23), 6206. https://doi.org/10.1039/c2sm25442e

Alouges2013 [29] Alouges, F., DeSimone, A., Giraldi, L., & Zoppello, M. (2013). Self-propulsion of slender micro-swimmers by curvature control: N-link swimmers. International Journal of Non-Linear Mechanics, 56, 132–141. https://doi.org/10.1016/j.ijnonlinmec.2013.04.012

Alouges2015 [30] Alouges, F., DeSimone, A., Giraldi, L., & Zoppello, M. (2015). Can Magnetic Multilayers Propel Artificial Microswimmers Mimicking Sperm Cells? Soft Robotics, 2(3), 117–128. https://doi.org/10.1089/soro.2015.0007

Khurshudyan2018 [31] Khurshudyan, A. Z. (2018). Min(max)imization of horizontal and vertical displacements of a fibre-reinforced magneto-elastic cantilever rod. ZAMM - Journal of Applied Mathematics and Mechanics / Zeitschrift Für Angewandte Mathematik Und Mechanik, 98(11), 1924–1929. https://doi.org/10.1002/zamm.201800192

Acharya2018 [32] Acharya, A. (2018). A Design Principle for Actuation of Nematic Glass Sheets. Journal of Elasticity. https://doi.org/10.1007/s10659-018-9696-z

Ciambella2018 [33] Ciambella, J., Favata, A., & Tomassetti, G. (2018). A nonlinear theory for fibre-reinforced magneto-elastic rods. Proceedings of the Royal Society A: Mathematical, Physical and Engineering Science, 474(2209), 20170703. https://doi.org/10.1098/rspa.2017.0703

CDGT2019 [34] Ciambella, J., Durastanti, R., Giacomelli, L., and Tomassetti, G. In preparation.

Hinze2008 [35] Hinze, M., Pinnau, R., Ulbrich, M., & Ulbrich, S. (2008). Optimization with PDE constraints. Springer Science & Business Media.

Troltszch2010 [36] Tröltzsch, F, (2010). Optimal control of partial differential equations: theory, methods, and applications. American Mathematical Soc.